

Three-dimensional dose-distribution measurement of therapeutic carbon-ion beams using a ZnS scintillator sheet

Katsunori Yogo^{1,*}, Masato Tsuneda², Ryo Horita¹, Hikaru Souda³,
Akihiko Matsumura³, Hiromichi Ishiyama², Kazushige Hayakawa²,
Tatsuaki Kanai³ and Seiichi Yamamoto¹

¹Graduate School of Medicine, Nagoya University, 1-1-20 Daiko-minami, Higashi-ku, Nagoya, Aichi 461-8673, Japan

²Graduate School of Medical Science, Kitasato University, Kanagawa 252-0373, Japan

³Gunma University Heavy Ion Medical Center, Gunma University, Gunma 371-8511, Japan

*Corresponding author. Katsunori Yogo, Graduate School of Medicine, Nagoya University, 1-1-20 Daiko-minami, Higashi-ku, Nagoya, Aichi 461-8673, Japan.
E-mail: yogo@met.nagoya-u.ac.jp; Fax: (81) 52-719-3172

(Received 14 October 2020; revised 19 January 2021; editorial decision 4 April 2021)

ABSTRACT

The accurate measurement of the 3D dose distribution of carbon-ion beams is essential for safe carbon-ion therapy. Although ionization chambers scanned in a water tank or air are conventionally used for this purpose, these measurement methods are time-consuming. We thus developed a rapid 3D dose-measurement tool that employs a silver-activated zinc sulfide (ZnS) scintillator with lower linear energy transfer (LET) dependence than gadolinium-based (Gd) scintillators; this tool enables the measurement of carbon-ion beams with small corrections. A ZnS scintillator sheet was placed vertical to the beam axis and installed in a shaded box. Scintillation images produced by incident carbon-ions were reflected with a mirror and captured with a charge-coupled device (CCD) camera. A 290 MeV/nucleon mono-energetic beam and spread-out Bragg peak (SOBP) carbon-ion passive beams were delivered at the Gunma University Heavy Ion Medical Center. A water tank was installed above the scintillator with the water level remotely adjusted to the measurement depth. Images were recorded at various water depths and stacked in the depth direction to create 3D scintillation images. Depth and lateral profiles were analyzed from the images. The ZnS-scintillator-measured depth profile agreed with the depth dose measured using an ionization chamber, outperforming the conventional Gd-based scintillator. Measurements were realized with smaller corrections for a carbon-ion beam with a higher LET than a proton. Lateral profiles at the entrance and the Bragg peak depths could be measured with this tool. The proposed method would make it possible to rapidly perform 3D dose-distribution measurements of carbon-ion beams with smaller quenching corrections.

Keywords: silver-activated zinc sulfide (ZnS); carbon-ion beam; linear energy transfer (LET); 3D dose distribution

INTRODUCTION

Carbon-ion beams are useful for treating tumors and offer physical dose localization and strong biological effects [1, 2]. The biological advantages of carbon-ion beams over photons and protons, which cannot be realized by simply increasing the dose, originate from their high linear energy transfer (LET) [2]. Measuring the 3D dose distribution of a carbon-ion beam is necessary for safe patient treatment. Precise measurements of the dose distribution of a carbon-ion beams are performed in regular quality assurance (QA) practice. Accurately measuring dose profiles and checking their consistency is essential

for QA in carbon-ion therapy. Monthly constancy tests of lateral dose profiles are recommended to check for variations from base lines in both photon and electron-beam therapy [3].

A rapid and reliable method for measuring the 3D dose distribution would be useful for QA in carbon-ion therapy. The measurement should have a sub-mm spatial resolution to measure the penumbra of the lateral profiles at the entrance and peak. It should also reproduce steeper dose distributions in the depth direction of carbon ions. The ratio of the dose at the Bragg peak to that at the entrance depth is typically approximately 5 and 3 for mono-energetic and spread-out

Bragg peak (SOBP) beams, respectively. In previous studies, ionization chambers that were scanned in water tanks were employed to measure the precise 3D dose distributions of carbon-ion beams [4–7]. Although these high-sensitivity chambers are suitable for measuring carbon-ion beams, the measurements of the depth- and lateral-dose profiles in this way is labor intensive. Gel dosimetry is another method for obtaining 3D dose distributions [8]. This method employs a radiation-induced chemical reaction. However, this method requires magnetic resonance imaging (MRI) or optical computed tomography (CT) equipment to interpret the data, and the pre-processing of the materials employed is time consuming.

Scintillators, on the other hand, offer a promising approach to conduct rapid 3D dose distribution measurements of carbon-ion beams. For example, gadolinium-based (Gd) scintillators are widely employed to measure the dose distributions of therapeutic protons [9–11]. These scintillators are also used in carbon-ion beam dosimetry [12–14]. However, for use in carbon-ion beam dosimetry, Gd scintillators require dose reconstruction and significant corrections [12]. Therefore, their application is limited to the entrance depth [13] and/or in air only [14] for carbon-ion beams. The LET of carbon ions is higher than that for protons [15, 16]. One problem associated with using a scintillator for carbon-ion beams is the light intensity dependence on the LET of the carbon ions.

A scintillator with lower LET dependence is desirable for measuring carbon-ion beams. It can provide 3D dose distribution measurements with smaller corrections. A silver-activated zinc sulfide (ZnS) scintillator was selected for carbon-ion beam dosimetry with a higher LET [17–19]. In a previous study, we proposed a ZnS scintillator for measuring dose profiles in high- and low-dose regions of carbon-ion pencil beams [20, 21]. This technique proved to be superior to methods employing a Gd-based scintillator in terms of LET. However, although optical imaging using a scintillator is a promising approach for obtaining dose-distribution measurements, the measured images are generally 2D.

In this study, we therefore employed a ZnS scintillator sheet combined with a water tank and a mirror to obtain optical images of 3D dose distributions. The ZnS sheet produced images of the carbon-ion beams. The images were reflected with a mirror to enable measurement using a charge-coupled device (CCD) camera from the side. By adjusting the water depth in the tank that was installed on the ZnS sheet, scintillation images of different depths were obtained. Three-dimensional dose images were created using the images captured at different depths by stacking them using computer software. The proposed method allows a more rapid measurement of the 3D dose distribution than previous methods. We compared the intensities of the created 3D images with the doses measured using an ionization chamber to assess the prospect of applying the proposed approach to carbon-ion therapy QA.

MATERIAL AND METHODS

3D dose distribution imaging system

A schematic view of the 3D dose measuring tool used in this study is shown in Fig. 1. The tool was composed of a ZnS scintillator, mirror and CCD camera, which were covered by a dark box (200 × 250 × 600 mm³). The box was set under a water tank (240 mm

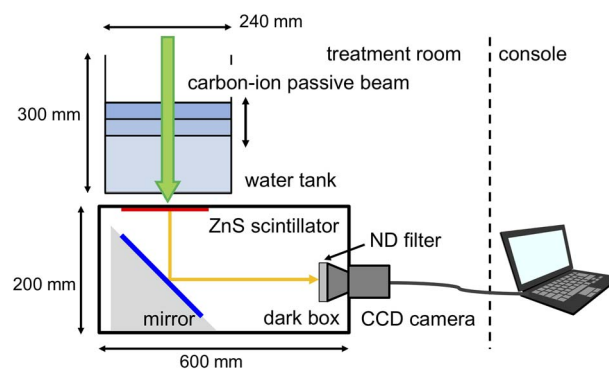


Fig. 1. Schematic of the imaging system used to measure the 3D dose distribution of the carbon-ion beam.

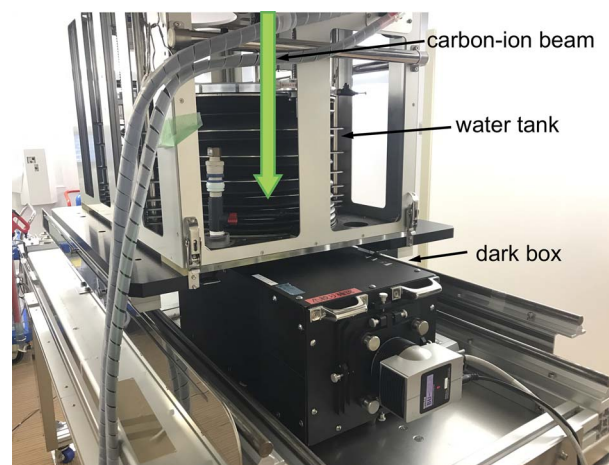


Fig. 2. Photograph of 3D carbon-ion beam imaging system (dark box and water tank).

diameter × 0–300 mm height) made from 10 mm-thick polymethyl methacrylate (PMMA). The water level in the tank was remotely regulated to change the measuring depth with 0.1 mm precision and was systematically adjusted to capture scintillation images at different depths. A photograph of the imaging system, including the water tank and the dark box, is shown in Fig. 2.

A ZnS scintillator sheet (150 × 150 mm², Mitsubishi-Kagaku, Tokyo, Japan) was supported on a black aluminum plate (0.6-mm water-equivalent thickness) and set vertical to the beam axis [17–22]. The scintillation light produced by carbon-ion beam irradiation was reflected by a mirror (at 45°) and detected with a CCD camera (BU-SOLN, BITRAN, Gyoda, Japan). The camera was set vertical to the beam axis and 450 mm from the scintillator. A lens (23FM16SP, Tamron, Saitama, Japan) was fixed at F = 1.4. The light intensity was adjusted by a neutral density (ND) filter [23].

The camera was remotely controlled by a personal computer from the console via a cable. Scintillation images were obtained by starting and ending with signals from an external control system (Accelerator Engineering Corp., Chiba, Japan). The typical exposure time of the camera was approximately 7 s with a peak dose of 2 Gy.

Carbon-ion beam delivery

All experiments were performed using carbon-ion beams delivered at the Gunma University Heavy Ion Medical Center, Gunma, Japan [24]. The scintillator was irradiated with 290 MeV/u mono-energetic carbon-ion beams with a field size of $80 \times 80 \text{ mm}^2$. A beam with a SOBP that had an $80 \times 80 \text{ mm}$ field and a 10-mm uniform physical dose field range was used. Carbon-ion beams were irradiated with a passive irradiation system consisting of wobbler magnets, scatterer, beam monitor and multi-leaf collimator (MLC) [24]. A ridge filter was used to deliver the SOBP beam. The irradiated carbon-ion beam used to acquire each image was approximately 4000 monitor counts, yielding 2 Gy at the Bragg peak for the mono-peaked passive beam. The water tank and dark box were aligned to the vertical beam line at the passive beam port. The box was set 27 mm below the water tank. The scintillator center was adjusted to the isocenter (source scintillator distance; 3564 mm).

For reference data, depth-dose profiles were measured with a plane-parallel chamber (TN3404S, PTW, Freiburg, Germany), which was installed on a plastic phantom (Tough Water, Kyoto Kagaku, Kyoto, Japan) and set under the water tank. To measure the lateral dose profiles (off-center ratio), the detector was scanned by remote control in the lateral direction with a 2 mm pitch. The black aluminum plate was placed above the chamber for consistency with the scintillation measurements.

Image processing and creation of 3D scintillation images

The recorded images were saved in 16-bit grayscale in the tagged image file format. The image size was 772×580 pixels, and the pixel size was 0.24 mm. The system distortion was less than one pixel [23]. The background images were acquired with the same exposure time without irradiation as the scintillation images.

The recorded images were processed using a public domain software (ImageJ, v.1.47, NIH) [23]. With the software, the background images were subtracted from the scintillation images and processed using a median filter with a 2 pixel radius [25]. The depths indicated the water-equivalent depths (WEDs), which included the bottom wall of the tank (11.6 mm of PMMA) and the black aluminum plate (0.6 mm) above the scintillator. Each 3D image was created from the corresponding measured 2D image using ImageJ [26]. To compensate the quenching effect (brightness reduction due to a higher LET), correction factors were multiplied to the brightness of the images at each depth. The correction factors were calculated as the signal ratio (ionization chamber / (ZnS scintillator)) at each depth in the depth profile. Because the original 2D images had different depth intervals, we interpolated the images with 1-mm intervals using linear interpolation. Through these procedures, we obtained 2D scintillation images with 1-mm intervals. These images were used to generate sagittal, coronal and volume-rendered images to demonstrate the usefulness of the 3D distribution of the scintillation images. The field sizes were evaluated as full width at half maximum (FWHM) in the lateral profiles.

RESULTS

Observed scintillation images

Figure 3a–c shows scintillation images of the mono-energetic 290 MeV/u carbon-ion beam obtained with the ZnS scintillator at three different

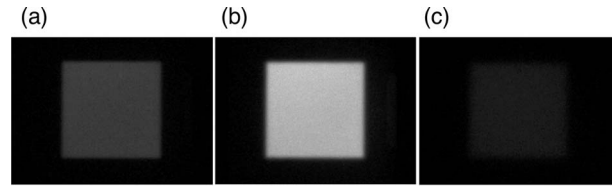


Fig. 3. Scintillation images of a passive beam at the (a) depth of the entrance (68.8 mm), (b) Bragg peak (138.8 mm), and (c) tail (141.6 mm) using a 290-MeV/u mono beam of carbon ions.

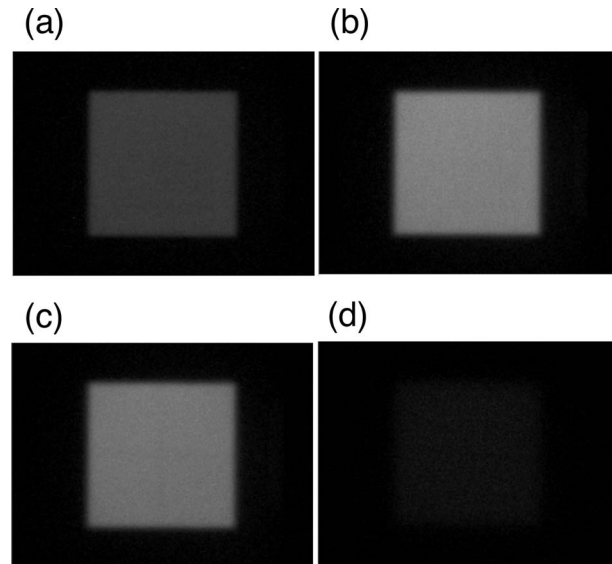


Fig. 4. Scintillation images of a mini-SOBP beam at the (a) depth of the entrance (65.2 mm), (b) center of the SOBP (135.2 mm), (c) edge of the SOBP (138.6 mm), and (d) tail (143.6 mm) using a 290-MeV/u mono beam of carbon ions.

depths: entrance (68.8 mm), Bragg peak (138.8 mm) and tail (141.6 mm). The highest intensity of the image is observed at the Bragg peak. The irradiated fields ($80 \times 80 \text{ mm}^2$) of the passive beam are observed as clear square spot images at the Bragg-peak depth (Fig. 3b) and entrance (Fig. 3a). In contrast, a dimmer image is observed at the tail depth (Fig. 3c).

Figure 4a–d shows scintillation images of the carbon-ion beam with SOBP measured using the ZnS scintillator at four different depths: entrance (65.2 mm), SOBP center (135.2 mm), SOBP edge (138.6 mm) and tail (143.6 mm). The image intensity at the SOBP center is similar to that at the SOBP edge and exceeds the intensity at the entrance. The image intensity at the tail shows a significantly lower brightness.

Depth profiles of measured scintillation images

Figure 5 depicts the depth profile of a 290 MeV/u mono carbon-ion beam measured by the ZnS scintillator. These depth profiles are compared with those measured using the ionization chamber. The depth profiles measured with the scintillator show a similar trend to

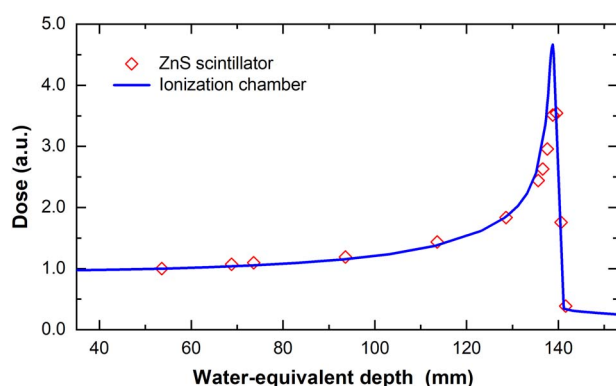


Fig. 5. Depth profiles measured using scintillation images for a mono-energetic beam (290 MeV/u). The data were compared with depth profiles measured with the ionization chamber.

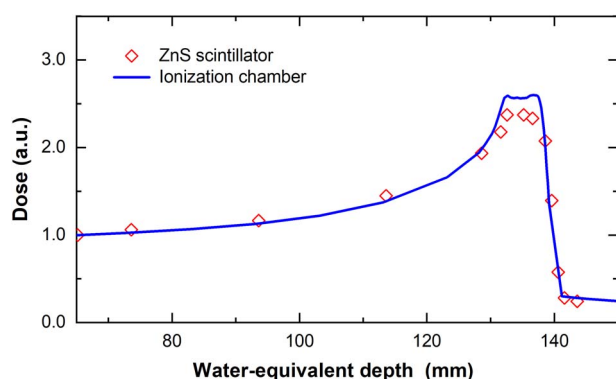


Fig. 6. Depth profiles measured using scintillation images for a uniform field with SOBP. The data were compared with the depth profiles measured with the ionization chamber.

those measured with the chamber, except around the Bragg peak. The scintillator underestimates the Bragg peak by approximately 20% in the case of the carbon-ion beam with a higher LET. The result is consistent with previously reported results for pencil beams (Fig. 5) [18, 20].

Figure 6 shows the depth profile of the carbon-ion beam with SOBP measured with the proposed ZnS scintillator. This depth profile is compared with those measured using the ionization chamber. The depth profile measured with the scintillator shows a similar trend to those measured with the chamber, except around the SOBP. The ZnS scintillator underestimates the SOBP center by approximately 10%, which is a significantly lower underestimation than that of the mono-energetic passive and pencil beams (Fig. 6) [18, 20].

Lateral profiles of measured scintillation images

Figure 7a and b shows the lateral profiles of a 290 MeV/u carbon-ion beam measured using the ZnS scintillator at two different depths: the entrance (68.8 mm) and Bragg peak (138.8 mm). The lateral profiles obtained with the ZnS scintillator are almost identical to the lateral dose profiles measured using the chamber, with a maximum difference of approximately 6% at the peak of the mono-energetic beam. These

tendencies are similar to those observed at the entrance (Fig. 7a) and at the Bragg peak (Fig. 7). The maximum difference in the FWHM of the field sizes in the lateral profiles obtained with the ZnS scintillator and with the chamber is 1.5 mm.

Figure 8a and b shows the lateral profiles of the carbon-ion beam with SOBP measured using the ZnS scintillator at two different depths: the entrance (65.2 mm) and Bragg peak (135.2 mm). The lateral profiles obtained by the ZnS scintillator are almost identical to the lateral dose profiles measured using the chamber, with a maximum difference of approximately 4%. These tendencies are similar to those observed at the entrance (Fig. 8a) and the Bragg peak (Fig. 8b). Again, the maximum difference in the FWHM of the field sizes in the lateral profiles obtained with the ZnS scintillator and with the chamber is 1.5 mm.

Sagittal slice of measured 3D scintillation images

Resliced sagittal images in the central slices from the 3D scintillation measurements for 290 MeV/u mono and SOBP carbon-ion beams are shown in Fig. 9a and b, respectively. Videos of the two sagittal images with their various slices are provided in the Supplementary Data (see Supplementary Data 1 and 2).

Volume-rendered 3D scintillation images

The created 3D scintillation images for the 290 MeV/u mono and SOBP carbon-ion beams are displayed in volume-rendered form in Fig. 10a and b, respectively. Three different views are shown in the figures. Three-dimensional images of the carbon-ion beam in water can be observed in different views. Videos of the volume-rendered 3D scintillation images of the mono-energetic and SOBP beams are provided in the Supplementary Data (see Supplementary Data 3 and 4).

DISCUSSION

Three-dimensional scintillation images of carbon-ion passive beams were successfully obtained using a ZnS scintillator and by changing the water depths (Figs 3, 4 and 10). Because a carbon-ion beam shows a much higher LET than a proton beam, when obtaining carbon-ion beam images, the scintillator has a LET-intensity dependency response. We thus employed the ZnS scintillator, instead of the Gd-based scintillators used in previous studies on therapeutic ion beams [9–14]. We previously reported that the ZnS scintillator provided a lower LET dependence on carbon ions than Gd-based scintillators [20]. Thus, ZnS scintillators require much smaller corrections than Gd scintillators in estimating dose distributions based on brightness distributions for carbon-ion pencil beams [20, 21].

The depth profiles of passive beams measured with the scintillation images obtained in this study were comparable to those measured by an ion chamber, except around the Bragg peak, where the errors were approximately 20% (Fig. 5). These differences could be the result of the quenching effects of the carbon-ion beam with a higher LET; the light intensity decreased due to the higher LET of the carbon ions [9]. The quenching effect can be explained by the following mechanisms [9]. For inorganic scintillators, high-energy charged particles produce electron–hole pairs, also called excitons. The recombination of these excitons with activator sites yields the scintillation. Quenching occurs when many excitons are produced by high LET particles and results in

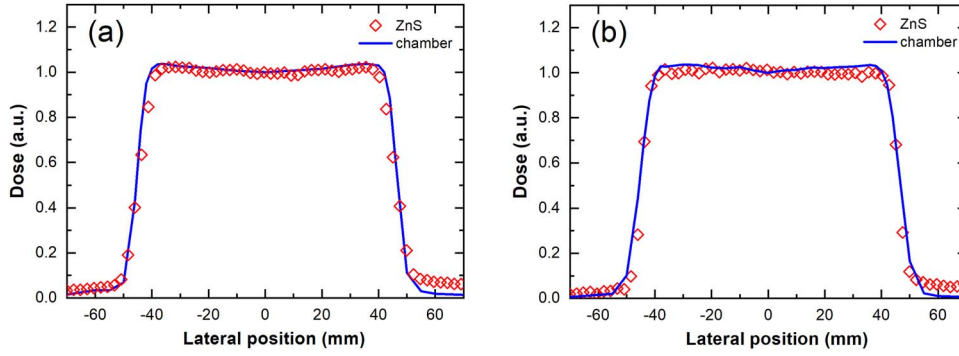


Fig. 7. Lateral profiles of a 290 MeV/u mono beam of carbon ions measured with the ZnS scintillator. The profiles were analyzed at the (a) entrance (68.8 mm), and (b) Bragg peak (138.8 mm). The data were compared with the lateral profiles measured with the ionization chamber. Profiles are normalized to their center value at each depth.

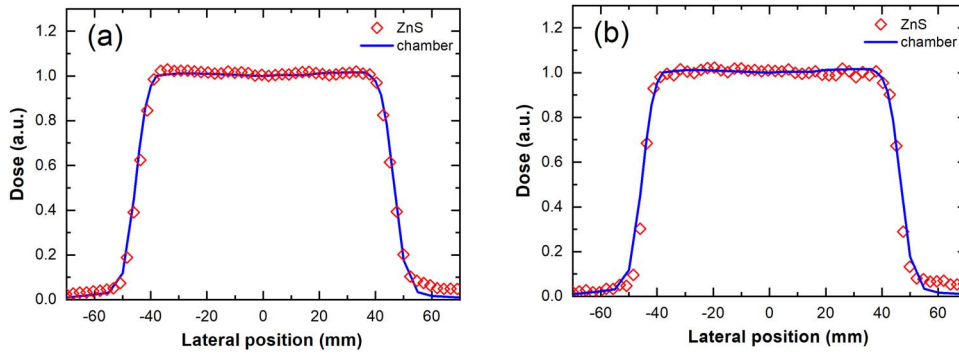


Fig. 8. Lateral profiles of an SOBP carbon-ion beam measured with the ZnS scintillator. The profiles were analyzed at the (a) entrance (65.2 mm), and (b) center of the SOBP (135.2 mm). The data were compared with the lateral profiles measured with the ionization chamber. Profiles are normalized to their center value at each depth.

the depletion of activator sites. These differences due to the quenching effect are similar to those reported in other studies on pencil beams [18, 20], and they are much smaller than those of the Gd scintillator, which produced an underestimation at the Bragg peak of approximately 40% [14, 20]. The differences between the scintillator and ion-chamber data for the SOBP beam are much smaller than those of the mono-energetic beam, which can be attributed to the smaller LET of the SOBP beams (Figs 5 and 6). Typical LETs for mono-energetic beams are in the range of 300–400 keV/ μm at the distal part of the Bragg peak [15]. Typical LETs for SOBP beams are in the range of 60–80 and 100–200 keV/ μm at the center region and end of the SOBP, respectively [15]. In this study, we compensated the quenching effect by multiplying the scintillator brightness by the correction factor (signal ratio \sim (ionization chamber) / (ZnS scintillator)) at each depth when creating the 3D images.

In the depth profiles of the carbon-ion pencil beam, the scintillator intensities were previously slightly higher than those of the chamber in the rising region of the Bragg peak [20]. However, this tendency was not observed in the depth profiles measured in this study; note that we used the same scintillator and chamber used in Yogo *et al.* [20] but with a passive beam and a larger field size (Figs 5 and 6).

Although these differences were not well understood, they were not due to the properties of the scintillators. They instead represented a decrease in the reference data signals. The beam spot size obtained in Yogo *et al.* [20] was comparable to the size of the detector that was used to measure the depth doses.

The lateral profile measured with the scintillator agreed with the lateral dose profiles measured with the chamber within approximately 4% for the SOBP beam at the depths of the entrance and Bragg peak (Fig. 8). The SOBP beam has much better alignment than the mono-energetic beam. The discrepancy between the lateral profiles slightly increases to approximately 6% at the depth of the Bragg peak in the case of the mono-energetic beam (Fig. 7b), which is due to the higher LET. We attributed these differences in the lateral-dose profiles, especially in the slope (spreading) at the edges, to the difference in the detector size, i.e. the spatial resolution of the measurements.

The right part of the profiles showed much larger systematic errors than the left part (Figs 7b and 8b). The systematic errors in the profiles in the right part are thought to be originated from the brightness decrease of the ZnS scintillator sheet. We found that the scintillation brightness in the ZnS sheet was not uniform (the deviation was within 10% for a $150 \times 150 \text{ mm}^2$ field), presumably resulting from the

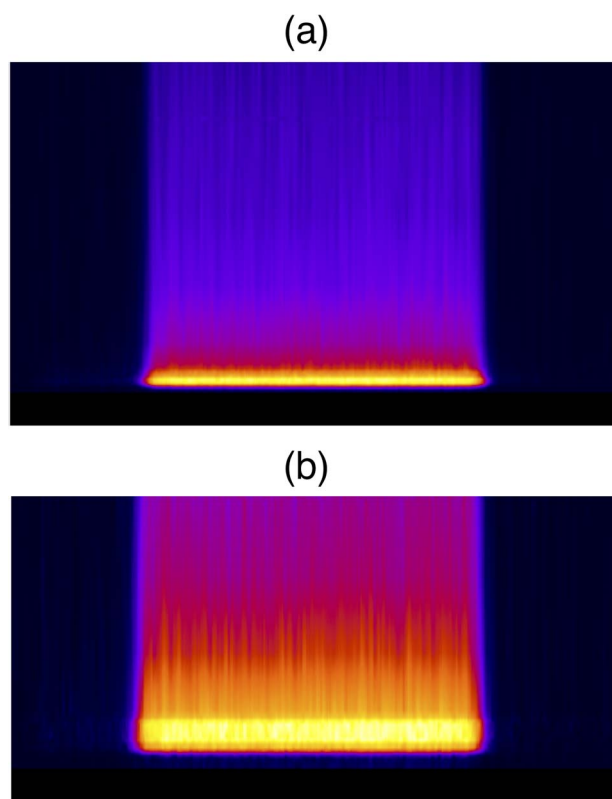


Fig. 9. Re-sliced sagittal scintillation images of the carbon-ion beam with (a) 290 MeV/u mono, and (b) SOBP beams.

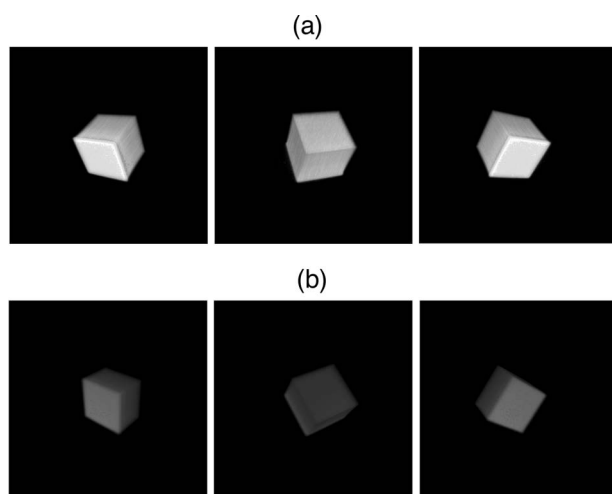


Fig. 10. Different views of volume-rendered 3D scintillation images for (a) 290 MeV/u mono, and (b) SOBP carbon-ion beams.

nonuniformity of the thickness of the phosphor layer. Therefore, we should compensate for the nonuniformity due to corrections such as the flat-field correction [12, 13].

The field sizes in the lateral profiles were evaluated using their FWHM. The FWHM for the data measured with the scintillator agreed to within 1.5 mm with those obtained using the chamber (Figs 7 and 8). This agreement of the ZnS profile with the chamber profiles is consistent with previous data for the pencil beam [20, 21].

Lateral profiles of the water (with the scintillator under the water tank) at the Bragg peak and entrance could be measured using the ZnS scintillator with small corrections, thereby showing its better performance in the 3D measurement of carbon-ion beams compared to Gd scintillators. Gd scintillators require reconstruction and large corrections to obtain the dose distribution [12] and can only be used at the entrance [13] and/or in air [14].

3D scintillation images of carbon-ion beams were successfully obtained by using the ZnS scintillator and changing the water depths (Fig. 10). With scintillation images obtained in the 3D data, we could construct depth and lateral profiles in any part of the images (Fig. 9). We used linear interpolation to construct images between the recorded images to obtain images with a 1 mm separation. Measuring scintillation images with smaller intervals and increasing the number of 2D images would provide smoother depth profiles with a certain corresponding increase in the total measurement time. Automatically changing the water depth for synchronization with the carbon-ion beam irradiation and the CCD camera exposure would also make the system more practical for the advanced 3D dose measurements of carbon-ion beams.

The proposed method allows a more rapid measurement of 3D dose distributions compared to the 3D scanning system method, which involved scanning the point detector with step-by-step methods in three directions (x, y, z-directions). Typically, the measurements, including those of the depth profile (0–140 mm with 1 mm pitch), lateral profiles at each depth (field size of $80 \times 80 \text{ mm}^2$ with 1 mm pitch) require approximately 120 min. In contrast, the proposed method with the scintillator sheet provided 3D images within typically 10 min (1 mm pitch in the depth direction, and 0.2 mm resolution in the lateral directions).

Carbon ion beams produce several types of secondary particles. The secondary particles produced by the SOBP beam could not be distinguished from primary carbon ions and appeared in the total dose measured with the ionization chamber, especially in the depth profile of the SOBP plateau. In this study, we corrected the scintillation brightness, including that produced by these particles, by multiplying it by a correction factor as follows: signal ratio \sim (ionization chamber) / (ZnS scintillator). However, further studies on the brightness response to these particles are necessary. Such studies should use each secondary particle as single primary beams.

CCD cameras can be damaged by a radiation field, and it is known that high-LET particles (including secondary neutrons) deteriorate the functions of CCD cameras. Therefore, in this study, we set installed the CCD camera away from the primary beam line (450 mm) to prevent the radiation damage of the camera. We used this system for over 5 years, but the CCD element did not get severely damaged. We did not observe differences between background images and images before and after irradiation, suggesting that the neutron activation did not affect the images under the conditions applied in this study.

Although the ZnS scintillator yielded smaller LET dependence (quenching effect) than the Gd scintillator for carbon ions, it still

required small corrections (maximum of approximately 20%) to obtain the correct 3D dose distributions for carbon ions. Previous studies reported that, for a proton beam with a lower LET, 3D dose distributions showed good agreement with those obtained using a float glass plate that had no quenching effect [26, 27]. The float glass provides the advantage of a light output—approximately 20 times higher than that of silica glass, which does not undergo proton quenching [28]. The float glass is a suitable for dose estimation, as it can produce a relatively high light output for protons without quenching.

To the best of our knowledge, no materials have been reported that exhibit no quenching of carbon-ion beams with high LET. For the case of carbon-ion beams, the development of a scintillator with both high sensitivity and low quenching is difficult. We provided a deep learning method to correct scintillation images for the quenching effect [29]. Briefly, after training a convolutional neural network model for carbon ions using dose distributions and scintillation images, we could predict the dose distributions from measured scintillation images using the trained model.

CONCLUSION

The results of this study showed that a ZnS scintillator with lower LET dependence and an imaging system are beneficial for the rapid measurement of the 3D dose distribution in carbon-ion therapy with smaller corrections compared to the conventional Gd-based scintillator. The ZnS-scintillator-measured depth profile agreed with the depth dose measured using an ionization chamber and was more accurate than that measured by the conventional Gd scintillator. The lateral profiles of the ZnS scintillator showed good agreement with those measured with the chamber; they had a spatial resolution of ~ 0.2 mm, which is sufficiently smaller than typical penumbra. Thus, our proposed method is promising for 3D dose measurement of carbon-ion beams used in therapy. It can reproduce sharp dose changes at Bragg peaks (~ 5 times larger than those at the entrance). Future studies on the development of quenching corrections, e.g. using deep learning, for the carbon ions are necessary to obtain dose profiles.

SUPPLEMENTARY DATA

Supplementary data is available at *RADRES Journal* online.

ACKNOWLEDGEMENTS

This work was performed as part of the Research Project with Heavy Ions at the Gunma University Heavy Ion Medical Center (GHMC). We would like to thank the GHMC staff for helpful discussions and providing us use of their facility, as well as the GHMC operators for their support during the experiments.

FUNDING

This work was supported by JSPS KAKENHI JP18K07679.

CONFLICT OF INTEREST

The authors declare they have no conflicts of interest.

REFERENCES

1. Tsujii H, Kamada T. A review of update clinical results of carbon ion radiotherapy. *Jpn J Clin Oncol* 2012;42:670–85.
2. Ohno T. Particle radiotherapy with carbon ion beams. *EPMA J* 2013;4:1–9.
3. Klein EE, Hanley J, Bayouth J et al. Task group 142 report: quality assurance of medical accelerators. *Med Phys* 2009;36:4197–212.
4. Kusano Y, Kanai T, Yonai S et al. Field-size dependence of doses of therapeutic carbon beams. *Med Phys* 2007;34:4016–22.
5. Schwaab J, Brons S, Fieres J et al. Experimental characterization of lateral profiles of scanned proton and carbon ion pencil beams for improved beam models in ion therapy treatment planning. *Phys Med Biol* 2011;56:7813–27.
6. Li Y, Zhu RX, Sahoo N et al. Beyond Gaussians: a study of single-spot modeling for scanning proton dose calculation. *Phys Med Biol* 2012;57:983–97.
7. Sawakuchi GO, Zhu XR, Poenisch F et al. Experimental characterization of the low-dose envelope of spot scanning proton beams. *Phys Med Biol* 2010;55:3467–78.
8. Maeyama T, Fukunishi N, Ishikawa K et al. Radiological properties of nanocomposite Fricke gel dosimeters for heavy ion beams. *J Radiat Res* 2016;57:318–24.
9. Boon SN, van Luijk P, Schippers JM et al. Fast 2D phantom dosimetry for scanning proton beams. *Med Phys* 1998;25:464–75.
10. Boon SN, van Luijk P, Böhringer T et al. Performance of a fluorescent screen and CCD camera as a two-dimensional dosimetry system for dynamic treatment techniques. *Med Phys* 2000;27:2198–208.
11. Pedroni E, Scheib S, Böhringer T et al. Experimental characterization and physical modelling of the dose distribution of scanned proton pencil beams. *Phys Med Biol* 2005;50:541–61.
12. Furukawa T, Saotome N, Inaniwa T et al. Delivery verification using 3D dose reconstruction based on fluorescence measurement in a carbon beam scanning irradiation system. *Med Phys* 2008;35:2235–42.
13. Takeshita E, Furukawa T, Inaniwa T et al. A fluorescent screen+CCD system for quality assurance of therapeutic scanned ion beams. *Nucl Instrum Methods Phys Res, Sect B* 2011;269:2936–40.
14. Russo S, Mirandola A, Molinelli S et al. Characterization of a commercial scintillation detector for 2-D dosimetry in scanned proton and carbon ion beams. *Phys Med* 2017;34:48–54.
15. Kanai T, Furusawa Y, Fukutsu K et al. Irradiation of mixed beam and design of spread-out Bragg peak for heavy-ion radiotherapy. *Radiat Res* 1997;147:78–85.
16. Paganetti H. Relative biological effectiveness (RBE) values for proton beam therapy. Variations as a function of biological endpoint, dose, and linear energy transfer. *Phys Med Biol* 2014;59:R419–72.
17. Saotome N, Furukawa T, Inaniwa T et al. *11th Eur Part Accel Conf* 2008;1830.
18. Hara Y, Furukawa T, Mizushima K et al. Development of a compact dose verification system using a fluorescent screen for carbon-ion therapy. *J Korean Phys Soc* 2016;69:1014–8.

19. Lee SH, Sunaguchi N, Hirano Y et al. A carbon CT system: how to obtain accurate stopping power ratio using a Bragg peak reduction technique. *Phys Med Biol* 2018;63:035025. <https://iopscience.iop.org/article/10.1088/1361-6560/aaa453>
20. Yogo K, Tatsuno Y, Souda H et al. Scintillator screen for measuring dose distribution in scanned carbon-ion therapy. *Radiat Meas* 2019;129:106207.
21. Yogo K, Tatsuno Y, Souda H et al. Scintillator screen for measuring low-dose halo in scanning carbon-ion therapy. *Radiat Meas* 2020a;133:106299.
22. Leo WR. *Techniques for Nuclear and Particle Physics Experiments*, 2nd edn. Berlin: Springer, 1994;106299, <https://doi.org/10.1016/j.radmeas.2020.106299>
23. Yogo K, Tatsuno Y, Tsuneda M et al. Practical use of a plastic scintillator for quality assurance of electron beam therapy. *Phys Med Biol* 2017;62:4551–70.
24. Ohno T, Kanai T, Yamadaet S et al. Carbon ion radiotherapy at the Gunma University heavy ion medical Center: New facility set-up. *Cancer* 2011;3:4046–60.
25. Yogo K, Matsushita A, Tatsuno Y et al. Imaging Cherenkov emission for quality assurance of high-dose-rate brachytherapy. *Sci Rep* 2020b;10:3572.
26. Horita R, Yamamoto S, Yogo K et al. Three-dimensional (3D) dose distribution measurements of proton beam using a glass plate. *Biomed Phys Eng Express* 2019;5:045033. <https://iopscience.iop.org/article/10.1088/2057-1976/ab169e>
27. Yamamoto S, Horita R, Toshito T et al. Imaging of the scintillation light of float and silica glasses during irradiation of radiations. *J Instrum* 2018;13:P10021–1. <https://iopscience.iop.org/article/10.1088/1748-0221/13/10/P10021>
28. Darafsheh A, Taleei R, Kassaei A et al. Proton therapy dosimetry using the scintillation of silica fibers. *Opt Lett* 2017;42:847–50.
29. Yabe T, Yamamoto S, Oda M et al. Prediction of dose distribution from luminescence image of water using a deep convolutional neural network for particle therapy. *Med Phys* 2020;47:3882–91.